ACS OMEGA

http://pubs.acs.org/journal/acsodf

Article

Fabrication and Characterization of a Highly Sensitive and Flexible Tactile Sensor Based on Indium Zinc Oxide (IZO) with Imprecise Data Analysis

Usama Afzal, Muhammad Aslam, Kanza Maryam, Ali Hussein AL-Marshadi, and Fatima Afzal*

Cite This: https://doi.org/10.1021/acsomega.2c04156

Read Online

ACCESS | Metrics & More | Article Recommendations

ABSTRACT: Tactile sensors are widely used in the electronic industry. In the following research work, we proposed a tactile sensor based on indium zinc oxide (IZO) electrodes and used neutrosophic statistics to analyze the capacitance and resistance of the tactile sensor. The tactile sensor was fabricated by depositing the IZO electrodes on a polycarbonate substrate (a thin layer). The IZO was characterized through X-ray diffraction (XRD), field emission scanning electron microscopy (FESEM), and ultraviolet−visible (UV−vis) spectroscopy techniques. The sensor's electrical properties were characterized using an LCR meter, i.e., capacitance and resistance were measured in intervals with respect to changes in the applied force on the sensor at 1 kHz operational frequency. The sensor expressed high sensitivity with quick response and recovery times. The sensor also expressed long-term stability. For the analysis of capacitance and resistance, two statistical approaches, i.e., classical and neutrosophic approaches, were applied, and the better analysis approach for the sensor was found.

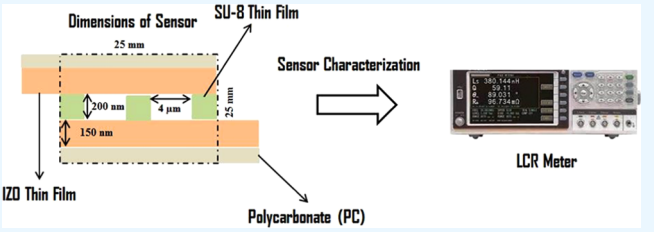

1. INTRODUCTION

The tactile sensor is an effective electronic instrument used for the tactile sensing of a human body,[1] robot skin,[2] tough screen devices,[3] etc. That is why there is a need to fabricate more effective and highly sensitive flexible tactile sensors with high response and recovery time. The tactile sensor senses the externally applied mechanical force's position and time and strength in the resolution of micron levels through the processing technology and produces useful data.[4] There are various sensing approaches used for developing tactile sensors such as capacitive type,[5] resistive type,[6] surface acoustic wave (SAW) type,[7] and optical using infrared (IR).[8] Numerous materials have been used in the fabrication of tactile sensors. Zhu et al. proposed a highly flexible and sensitive tactile sensor using porous graphene.[9] They used this sensor to observe the motion of the human body. Magnetron sputtering, photo-etching, and screen printing techniques were used in the fabrication of the tactile sensor, and they observed 60% strain recovery capability with high piezoresistive sensitivity. Similarly, Lü and his company fabricated an ultrahigh-sensitive tactile sensor based on a graphene thin film through the piezoresistivity technique for robotic biomedical applications.[10] They found the high sensitivity of sensors of about 10.80 Ω/kPa in the range of applied force of 0−4 kPa. Jiang et al. explored and proposed a flexible tactile sensor based on the nanocomposite material.[11] They used $BaTiO_3$/Poly (vinylidene fluoride) electrospun based on a nanocomposite membrane. Xie et al. proposed a highly flexible tactile sensor for the electronic/E-skin based on cellulose and carbon nanotube composite films.[12] They obtained a highly flexible tactile sensor of strength 61.6 MPa with 17.7% strain recovery. A highly sensitive capacitive-type tactile sensor with high resolution and ultrabroad range-based composite material carbon nanotube (CNT)/poly(dimethylsiloxane) (PDMS) thin film was proposed.[5] They found a high sensitivity of 1.61% kPa^{-1} and 0.9 kPa−2.55 MPa ultrabroad range. Moreover, Rosle et al. proposed the carbon nanotube−poly(dimethylsiloxane)−gel (CNT-PDMS)-Gel composite thin film-based tactile sensor.[13] In this way, researchers have used numerous materials in the fabrication of flexible and highly sensitive tactile sensors. Generally, it is seen that the measured data of the tactile sensor has been analyzed using statistics.

Single/fixed point data are analyzed through the classical formulas of statistics. However, for the interval data, classical approaches or formulas fail to properly analyze the data. Therefore, we would have to move to some new and novel statistics approach, i.e., neutrosophic statistics[14] proposed by Smarandache. Neutrosophic statistics is a more effective and

Received: July 2, 2022
Accepted: August 18, 2022

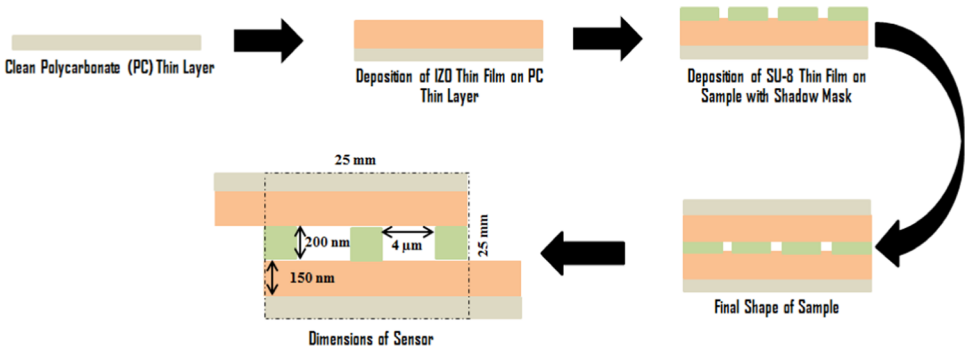

Figure 1. Schematic diagram of the tactile sensor.

informative approach for dealing with interval values. As it analyzes the data interval with respect to its indeterminate interval, i.e., there is no loss of indeterminacy of the interval. Nowadays, the use of neutrosophic statistics in materials science has increased (as you can see in our previous work).[15] The researchers used statistical approaches to analyze the interval data of resistance with respect to the change in the temperature of a conductor. They used both classical and neutrosophic statistics for analysis. Similarly, the classical and neutrosophic approaches were used to analyze the resistance and capacitance data of a humidity sensor based on methyl green; see refs 16−19. Through previous work, we have found that neutrosophic statistics is more reliable in the analysis of the interval data.

This study reports inspired work on the fabrication of a flexible tactile sensor based on indium zinc oxide (IZO) electrodes. The IZO electrodes are deposited on the polycarbonate thin layer through a thermal evaporator. The structure, surface, and optical properties of the IZO electrodes have been studied through X-ray diffraction (XRD), field emission scanning electron microscopy (FESEM), and ultraviolet−visible (UV−vis) spectroscopy techniques. For the first time, we have used an LCR meter for observing the electric properties of the tactile sensor by measuring the capacitance and the resistance simultaneously with respect to change in the applied force. The measured data are analyzed through the classical and neutrosophic approaches.

2. EXPERIMENTAL SECTION

In this work, we have fabricated a transparent capacitive- and resistive-type tactile sensor. The fabrication and characterization of the sensor are as follows:

2.1. Fabrication. First of all, two thin layers of polycarbonate (PC) were cleaned by washing them in acetone and deionized water. After that, these layers were dried through a nitrogen gun. Then, we deposited a thin layer of indium zinc oxide (IZO) having a thickness of 150 nm on both PC thin layers through a thermal evaporator at a pressure of about 10^{-5} bar.[20] A thin film having a thickness of 200 nm of an insulator photoresist material, i.e., SU-8 (eight epoxy groups) was deposited on one PC thin layer through spin coating with a shadow mask, and then, the other PC thin layer was put on it as shown in Figure 1. In this way, we fabricated a sample of the tactile sensors with dimensions of 25 × 25 mm^2.

2.2. Characterization. The indium zinc oxide structure was characterized through X-ray diffraction, the surface morphology was studied through field emission scanning electron microscopy, and the optical properties, i.e., transmission and absorption were studied through UV−visible spectroscopy. Then, we observed the electrical properties of the sensor by measuring the capacitance and resistance (in intervals, i.e., the maximum and minimum value of capacitance and resistance of the tactile sensor at a specific value of applied force) of the sensor in the lab. The capacitance and resistance were measured using an LCR meter at 1 kHz with respect to change in the applied force on the sensor through a force gauge, as shown in Figure 2. The measured data were analyzed

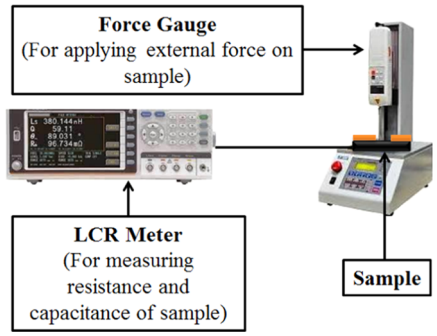

Figure 2. Characterization setup of the tactile sensor.

through classical and neutrosophic methods of statistics. The experiment was performed at the room temperature level, i.e., 22 °C, and the experiment was repeated four times and a minor variation was observed, i.e., 0.5−1.5%, which can be neglected.

3. RESULTS AND DISCUSSION

The XRD pattern (obtained through the Cu Kα X-ray source) of IZO is shown in Figure 3a. Six peaks are observed with the JCPDS card file 36-1451,[21] which show the hexagonal wurtzite crystal structure nature of the IZO. The peak (100) is observed at 31.84° with a *d*-spacing of 2.81 Å, (002) is observed at 34.46° with *a d*-spacing of 2.60 Å, (101) is observed at 36.33° with *a d*-spacing of 2.47 Å, (102) is observed at 47.54° with a *d*-spacing of 1.91 Å, (110) is observed at 31.84° with *a d*-spacing of 1.62 Å, and (103) is observed at 62.88° with *a d*-spacing of 1.47 Å. Similarly, the FESEM micrograph of IZO is shown in Figure 3b. It is seen that IZO electrodes have a smooth surface. However, there are some white dots on the surface, which help in the transmission of light.

The optical properties based on transmission and absorption of IZO have been studied by UV−visible spectroscopy, as shown in Figure 4. The transmittance and absorbance have been observed in the visible region of the light with the range

https://doi.org/10.1021/acsomega.2c04156
ACS Omega XXXX, XXX, XXX−XXX

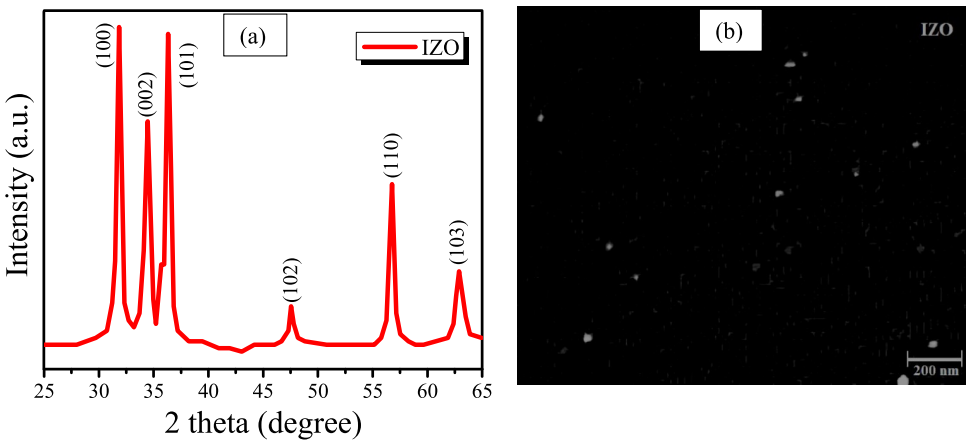

Figure 3. (a) XRD pattern of indium zinc oxide and (b) FESEM of indium zinc oxide.

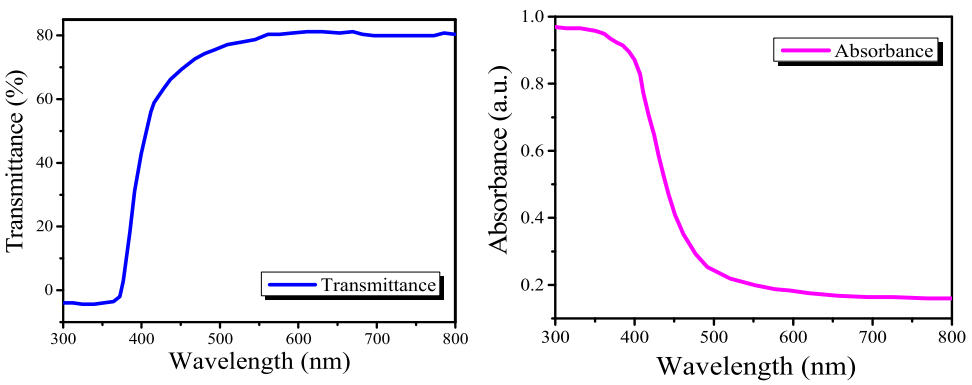

Figure 4. UV−vis spectroscopy analysis.

of 300−800 nm.[22] It is seen that the absorbance of the sample has decreased with respect to the increase in the wavelength of light, but transmittance has increased (81% transmittance observed). This means that transmittance and absorbance of the sample have an inverse relationship.[23]

Similarly, the capacitance and resistance of the tactile sensor measured through an LCR meter with respect to change in the applied force are shown in Table 1.

3.1. Effect of the Applied Force on Capacitance and Resistance. From Table 1 given above, it is seen that the capacitance of the sensor is increased as the applied force increases on the sensor. Basically, the dielectric microstructure of the material plays a very important role in the increase in the capacitance of the tactile sensor.[24] The capacitance of the sensor can be written as

$$C = \varepsilon_0 \varepsilon_r \frac{A}{d} \quad (1)$$

Here, "C" is the capacitance of the sensor, "ε_0" is the electric constant, "ε_r" is the relative permittivity, and "A" is the area of the electrodes. Generally, the value of relative permittivity depends on the nature of the material. A material having more relative permittivity is always preferred in the capacitive-type tactile sensor. Moreover, the distance between the electrodes represents the thickness of the dielectric material. As the force is applied, the thickness of the dielectric material is deformed and starts to decrease. As a result, the capacitance of the sensor is increased as shown in Table 1; the capacitance of the sensor is increased from 0.62 to 6.23 pF with respect to the applied force of 0−0.7 N. Similarly, it is observed that the resistance of the sensor has decreased as the applied force increased. The resistance of a sensor can be written as[16,19]

$$R = \frac{lA}{\alpha} \quad (2)$$

Table 1. Measured Capacitance and Resistance of the Tactile Sensor

force (N)	capacitance (pF)	resistance (kΩ)
0	[0.62, 1.14]	[875, 1626]
0.025	[1.35, 1.96]	[509, 742]
0.05	[2.14, 2.96]	[338, 467]
0.075	[3.05, 3.54]	[282, 328]
0.1	[3.49, 4.28]	[233, 286]
0.125	[4.02, 4.60]	[217, 249]
0.15	[4.19, 4.77]	[209, 238]
0.175	[4.31, 4.92]	[203, 232]
0.2	[4.39, 5.10]	[196, 227]
0.25	[4.72, 5.30]	[188, 212]
0.3	[4.86, 5.42]	[184, 205]
0.35	[4.92, 5.45]	[183, 203]
0.4	[5.01, 5.62]	[177, 199]
0.45	[4.89, 5.77]	[173, 204]
0.5	[4.83, 6.03]	[165, 206]
0.55	[4.92, 6.06]	[164, 203]
0.6	[5.04, 6.09]	[164, 198]
0.65	[5.05, 6.19]	[161, 198]
0.7	[5.15, 6.23]	[160, 194]

https://doi.org/10.1021/acsomega.2c04156
ACS Omega XXXX, XXX, XXX−XXX

Here, "R" is the resistance of the sensor, "A" is the area of the electrodes, "l" is the length of the deposited material between the electrodes, and "α" is the conductivity of the material of electrodes. The force is applied on the sensor, the electrodes start to compress and the atoms/molecules of the material through which the electrodes are fabricated become closer, which increases the conductance of the electrodes. As a result, the resistance of the sensor starts to decrease as shown in the table; the resistance for the said sensor has decreased from 1626 to 160 kΩ as the force is applied from 0 to 0.70 N.

Similarly, the effect of the dielectric layer (SU-8) on the sensor performance can be seen in Figure 5. It is observed that with an increase in the thickness of the dielectric layer, the capacitance is decreased but the resistance is increased.

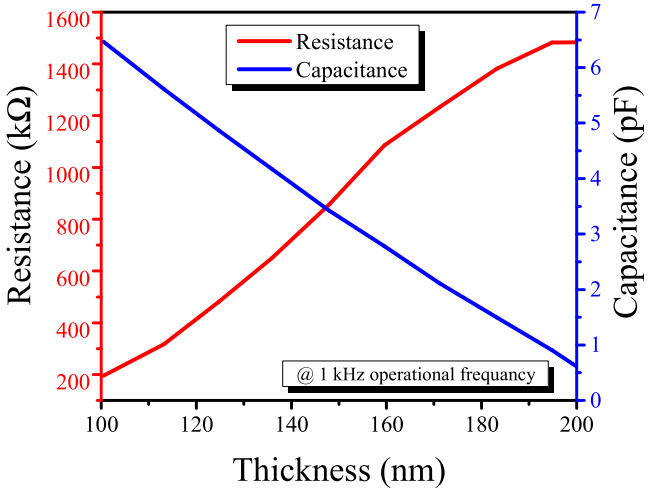

Figure 5. Effect of the dielectric layer on the sensor performance.

3.2. Response and Recovery Times. Response and recovery times of tactile sensors have been estimated through the dynamical investigation procedure. Figure 6 shows the graphs of the response and recovery times. The dynamical investigation has been implemented between two values of applied force, i.e., the low value is 0 N and the high value is 0.6 N. Sharp response and recovery times have been observed, i.e., 3.2 and 2.8 s, respectively.

3.3. Sensitivity and Long-Term Stability of the Tactile Sensor. Sensitivity is an important factor of the sensor. The sensitivity of the tactile sensor has been measured by the following formula

$$S = \left| \frac{R_{max}/C_{max} - R_{min}/C_{min}}{F_{max} - F_{max}} \times 100 \right| \quad (3)$$

"C_{max}" and "R_{max}" are the maximum measured values of capacitance and resistance, respectively, "C_{min}" and "R_{min}" are the minimum measured values of capacitance and resistance, respectively, "F_{max}" is the maximum applied force, and "F_{min}" is the minimum applied force. Thus, the sensitivity of tactile resistance is about 2.09 MΩ/N and that of capacitance is about 8.01 pF/N.

Similarly, the long-term stability of the tactile sensor has been checked for 30 days, as shown in Figure 7. It is seen that the sensor has expressed long-term stability with minor change in capacitance (which can be neglected).

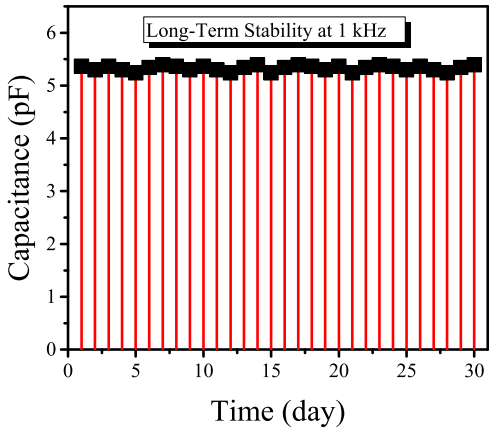

Figure 7. Long-term stability graph.

3.4. Analysis of Capacitance and Resistance. For the analysis of the interval data, the classical average or mean formula is used. Generally, it is seen that most researchers have used the classical average for interval data as can be seen in our previous research work,[17,18] which is as follows

$$M = \frac{X_L + X_U}{2} \quad (4)$$

Here, X_L is the minimum/lower value and X_U is the maximum/upper value of the interval. However, the neutrosophic one is

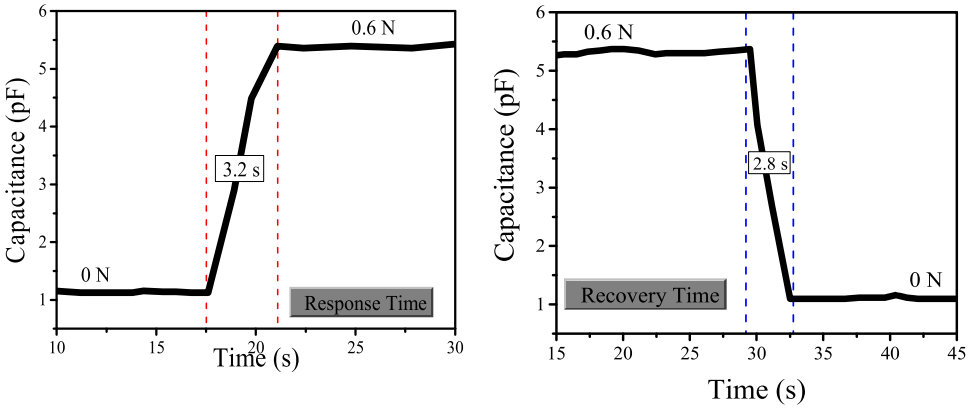

Figure 6. Response and recovery time of the tactile sensor.

https://doi.org/10.1021/acsomega.2c04156
ACS Omega XXXX, XXX, XXX−XXX

Table 2. Classical and Neutrosophic Analysis of the Measured Data

	capacitance (pF)		resistance (kΩ)	
force (N)	classical	neutrosophic	classical	neutrosophic
0	0.8785 ± 0.26	0.62 + 1.14I_N; $I_N \epsilon$ [0, 0.462]	1250.837 ± 375.2	875 + 1626I_N; $I_N \epsilon$ [0, 0.462]
0.025	1.6545 ± 0.31	1.35 + 1.96I_N; $I_N \epsilon$ [0, 0.314]	626.0372 ± 116.4	509 + 742I_N; $I_N \epsilon$ [0, 0.314]
0.05	2.548 ± 0.41	2.14 + 2.96I_N; $I_N \epsilon$ [0, 0.277]	402.8966 ± 64.8	338 + 467I_N; $I_N \epsilon$ [0, 0.277]
0.075	3.295 ± 0.25	3.05 + 3.54I_N; $I_N \epsilon$ [0, 0.141]	305.2332 ± 23.1	282 + 328I_N; $I_N \epsilon$ [0, 0.141]
0.1	3.8805 ± 0.40	3.49 + 4.28I_N; $I_N \epsilon$ [0, 0.185]	260.4037 ± 26.5	233 + 286I_N; $I_N \epsilon$ [0, 0.185]
0.125	4.3055 ± 0.29	4.02 + 4.60I_N; $I_N \epsilon$ [0, 0.127]	233.338 ± 15.9	217 + 249I_N; $I_N \epsilon$ [0, 0.127]
0.15	4.481 ± 0.29	4.19 + 4.77I_N; $I_N \epsilon$ [0, 0.123]	224.1227 ± 14.7	209 + 238I_N; $I_N \epsilon$ [0, 0.123]
0.175	4.613 ± 0.31	4.31 + 4.92I_N; $I_N \epsilon$ [0, 0.125]	217.7494 ± 14.3	203 + 232I_N; $I_N \epsilon$ [0, 0.125]
0.2	4.7445 ± 0.35	4.39 + 5.10I_N; $I_N \epsilon$ [0, 0.138]	211.9336 ± 15.7	196 + 227I_N; $I_N \epsilon$ [0, 0.138]
0.25	5.008 ± 0.29	4.72 + 5.30I_N; $I_N \epsilon$ [0, 0.111]	200.3664 ± 11.7	188 + 212I_N; $I_N \epsilon$ [0, 0.111]
0.3	5.14 ± 0.28	4.86 + 5.42I_N; $I_N \epsilon$ [0, 0.103]	195.1233 ± 10.6	184 + 205I_N; $I_N \epsilon$ [0, 0.103]
0.35	5.1845 ± 0.26	4.92 + 5.45I_N; $I_N \epsilon$ [0, 0.097]	193.3822 ± 9.8	183 + 203I_N; $I_N \epsilon$ [0, 0.097]
0.4	5.3155 ± 0.31	5.01 + 5.62I_N; $I_N \epsilon$ [0, 0.109]	188.7608 ± 10.9	177 + 199I_N; $I_N \epsilon$ [0, 0.109]
0.45	5.331 ± 0.44	4.89 + 5.77I_N; $I_N \epsilon$ [0, 0.153]	188.8687 ± 15.6	173 + 204I_N; $I_N \epsilon$ [0, 0.153]
0.5	5.433 ± 0.60	4.83 + 6.03I_N; $I_N \epsilon$ [0, 0.199]	186.3329 ± 20.6	165 + 206I_N; $I_N \epsilon$ [0, 0.199]
0.55	5.492 ± 0.57	4.92 + 6.06I_N; $I_N \epsilon$ [0, 0.188]	184.0728 ± 19.1	164 + 203I_N; $I_N \epsilon$ [0, 0.188]
0.6	5.565 ± 0.53	5.04 + 6.09I_N; $I_N \epsilon$ [0, 0.173]	181.3206 ± 17.2	164 + 198I_N; $I_N \epsilon$ [0, 0.173]
0.65	5.6195 ± 0.57	5.05 + 6.19I_N; $I_N \epsilon$ [0, 0.185]	179.8115 ± 18.3	161 + 198I_N; $I_N \epsilon$ [0, 0.185]
0.7	5.683 ± 0.53	5.15 + 6.23I_N; $I_N \epsilon$ [0, 0.171]	177.525 ± 16.6	160 + 194I_N; $I_N \epsilon$ [0, 0.171]

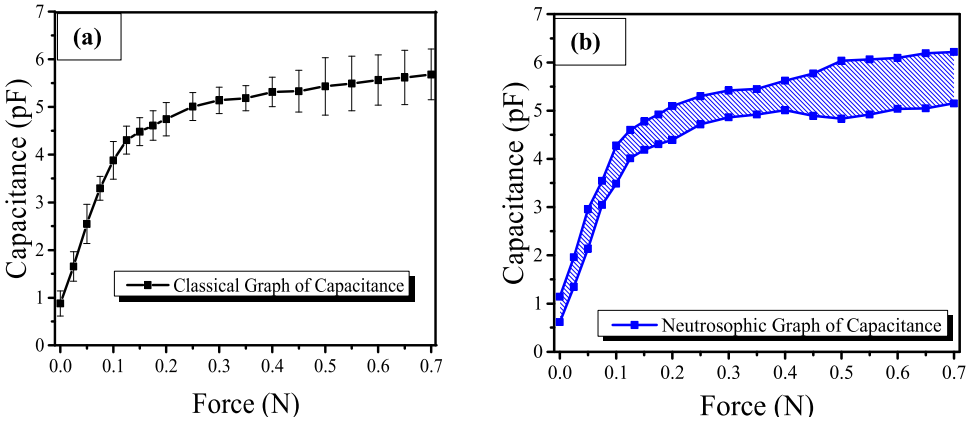

Figure 8. (a) Classical graph of capacitance and (b) neutrosophic graph of capacitance.

more generalized than the classical method; it deals with indeterminacy. For developing the neutrosophic formula for the analysis of the tactile sensor data, let us see some previous definitions of neutrosophic statistics. Let X_N be a neutrosophic variable with the interval of variance $X_N \epsilon [X_L, X_U]$ having size $n_N \epsilon [n_{NL}, n_{NU}]$ with indeterminacy $I_N \epsilon [I_{NL}, I_{NU}]$ and the neutrosophic formula can be written as follows[15]

$$X_{iN} = X_{iL} + X_{iU} I_N (i = 1, 2, 3, ..., n_N) \quad (5)$$

$X_{iN} \epsilon [X_{iL}, X_{iU}]$ has two parts: X_{iL} expressing the lower value which is under classical statistics and X_{iU} I_N being an upper part with indeterminacy $I_N \epsilon [I_L, I_U]$. Moreover, for intervals, the lower value of the indeterminacy interval is always taken as zero under classical statistics extension, i.e., $I_L = 0$. However, the upper value of the indeterminacy interval can be found by $I_U = [(X_{iU} - X_{iL})/X_{iU}]$. In this regard, the indeterminacy interval with respect to each is $I_N \epsilon [0, (X_{iU} - X_{iL})/X_{iU}]$. Similarly, the neutrosophic mean interval $[\bar{X}_N \epsilon \bar{X}_L, \bar{X}_U]$ is defined as follows

$$\bar{X}_N = \bar{X}_L - \bar{X}_U I_N; I_N \epsilon [I_L, I_U] \quad (6)$$

where $\bar{X}_L = \sum_{i=1}^{nU} \left(\frac{X_{iL}}{n_L}\right)$ is the lower value of the neutrosophic mean and $\bar{X}_U = \sum_{i=1}^{nU} \left(\frac{X_{iU}}{n_U}\right)$ is the highest value of the neutrosophic mean with the indeterminacy interval $I_N \epsilon [I_L, I_U]$. The neutrosophic formulas for capacitance $[C_L, C_U]$ and resistance $[R_L, R_U]$ are as follows

$$R_N = R_L + R_U I_N; I_N \epsilon [I_L, I] \quad (7)$$

$$C_N = C_L + C_U I_N; I_N \epsilon [I_L, I_U] \quad (8)$$

Now, we move to the analysis of the measured interval data of capacitance and resistance of the tactile sensor. For this proposal, we follow the procedure as in the methodology section. For example, for the first interval of capacitance [0.62, 1.14] at 0 N force as shown in Table 1, the classical value analyzed is 0.88 pF, which is calculated from the classical formula as shown in eq 4. Similarly, the value calculation of the same interval by neutrosophic analysis can be performed by the equation $C_{(0\ N)} = 0.62 + 1.14 I_N$ with the indeterminacy interval $I_N \epsilon [0, 0.461]$. According to neutrosophic analysis, the value of capacitance lies between 40.44 and 60.44 by applying

https://doi.org/10.1021/acsomega.2c04156
ACS Omega XXXX, XXX, XXX−XXX

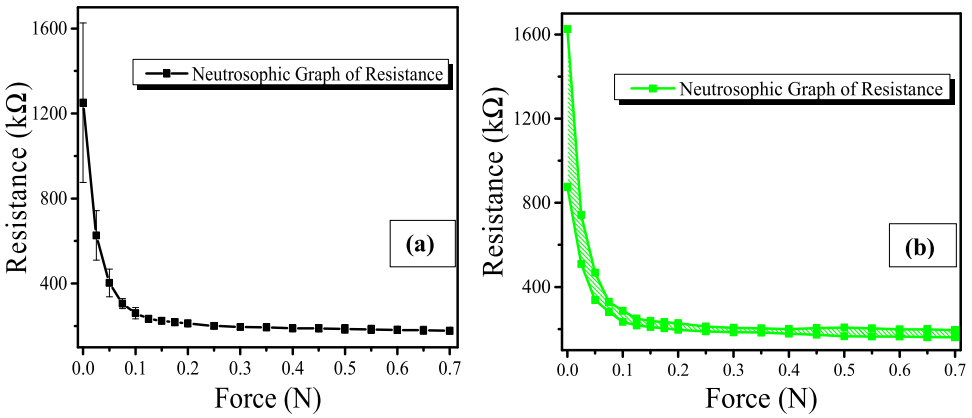

Figure 9. (a) Classical graph of resistance and (b) neutrosophic graph of resistance.

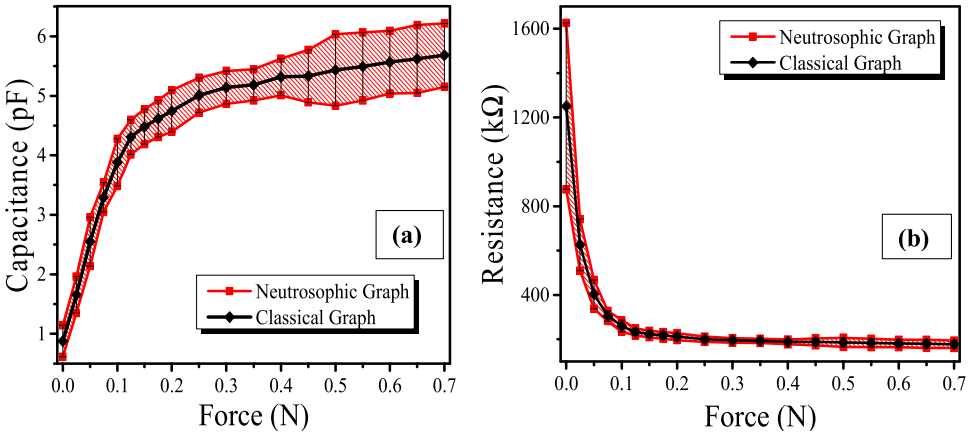

Figure 10. (a) Combined classical and neutrosophic graph for capacitance and (b) combined classical and neutrosophic graph for resistance.

Table 3. Difference between Classical and Neutrosophic Methods

classical method	neutrosophic method
the classical formula only provides a single value for an interval	the neutrosophic formula provides an equation that deals with indeterminacy of an interval
through this method, the interval loses its indeterminacy	this method does not affect the indeterminacy of the interval
it uses single-line or error bar graphs	it uses neutrosophic graphs that cover the whole variation of data
classical analysis is limited to classical statistics	neutrosophic analysis also defined the classical analysis, as neutrosophic statistics is the generalization of classical statistics
for example, according to the classical method, a statement is only true or only false at a time	for example, according to the neutrosophic method, a statement may be true or false at a time based on its indeterminacy interval

indeterminacy values. Similarly, the analysis of whole data is shown in Table 2.

Table 2 shows the classical and neutrosophic analysis of the measured interval data of resistance and capacitance. It is observed that the classical method has only provided the single values/fix-point values with some error for capacitance and resistance of the tactile sensor with respect to the applied force on the sensor. All the output values of classical analysis are based on the classical mean formula. However, the neutrosophic method has provided an equation for each data interval with its indeterminate interval. Through the indeterminate interval, a researcher can observe complete variation for each interval of capacitance and resistance.

Now, let us move to draw the calculated values of the capacitance and resistance of the tactile sensor through the classical and neutrosophic analysis. For capacitance, the classical and neutrosophic graphs are shown in Figure 8a,b, respectively. Also, for resistance, the classical and neutrosophic graphs are shown in Figure 9a,b, respectively.

From the above-given Figures 8 and 9, it is clearly seen that we have used error graphs in the classical approach (as general research has used such graphs to express the variation of data in the work[25−27]) for capacitance and resistance values. However, it is not much flexible and informative because the graphs only show the uncertainty of data. On the other hand, the present work contains a neutrosophic graph, which is more flexible and informative. This describes the whole capacitance and resistance variation with respect to changes in the applied force. The analysis methods and formulas of neutrosophic statistics are suitable for analysis.

3.4.1. Comparison. For the comparative study, we draw combined graphs of classical and neutrosophic graphs for the capacitance and resistance of the tactile sensor as shown in Figure 10a,b, respectively.

The first thing observed from Figure 10a,b is that the capacitance of the tactile sensor increases and the resistance decreases as the applied force increases. Moreover, the difference from the combined graphs of the classical and

https://doi.org/10.1021/acsomega.2c04156
ACS Omega XXXX, XXX, XXX−XXX

neutrosophic analysis can be seen in Table 3.[17,18,28] From the graphs, it is easily observed that neutrosophic statistics is the generalization of classical statistics, as the classical graphs fall in the middle of the neutrosophic graphs. Also, the neutrosophic graph is much more reliable in making decisions and in concluding the solution of the problem. The classical graphs only define the variation against a single value, but the neutrosophic graphs show the variation of the whole interval. Therefore, as a result, it can be concluded that the neutrosophic approach is flexible, informative, and reliable in the analysis of sensing data.[18,29]

4. CONCLUSIONS

The work explores the fabrication of tactical sensors with data analysis with different statistical approaches. Capacitive- and resistive-type tactile sensors have been fabricated by depositing indium zinc oxide (IZO) electrodes on the cleaned flexible polycarbonate layers with the help of a thermal evaporator at 10^{-5} bar. The structure of IZO has been characterized through XRD and found to have a hexagonal wurtzite crystal nature. The surface morphology has been examined by FESEM. UV−visible spectroscopy has been used for observing the optical properties. The capacitance and resistance of the sensor are measured in intervals using an LCR meter at 1 kHz. It is observed that the capacitance of the sensor increases as the applied force increases. However, the resistance decreases. The fabricated sensor showed a high response and recovery times, i.e., 3.2 and 2.8 s, respectively. The tactile sensor also expressed high sensitivity, i.e., resistance is about 2.09 MΩ/N and capacitance is about 8.01 pF/N. For analyzing the interval data, classical and neutrosophic approaches have been used. We have compared the methods and results of both approaches. As the result, it is concluded that the neutrosophic approach is more flexible, accurate, and informative in the analysis of the interval data compared to the classical approach.

AUTHOR INFORMATION

Corresponding Author

Fatima Afzal − *School of Chemistry, University of the Punjab, Lahore 54590, Pakistan*; Email: f.afzal.edu@gmail.com

Authors

Usama Afzal − *School of Microelectronics, Tianjin University, Tianjin 300072, China*; orcid.org/0000-0002-4039-0627

Muhammad Aslam − *Departments of Statistics, Faculty of Science, King Abdulaziz University, Jeddah 21551, Saudi Arabia*; orcid.org/0000-0003-0644-1950

Kanza Maryam − *School of Chemistry, University of the Punjab, Lahore 54590, Pakistan*

Ali Hussein AL-Marshadi − *Departments of Statistics, Faculty of Science, King Abdulaziz University, Jeddah 21551, Saudi Arabia*

Complete contact information is available at: https://pubs.acs.org/10.1021/acsomega.2c04156

Notes

The authors declare no competing financial interest.

ACKNOWLEDGMENTS

The authors are deeply thankful to the editor and reviewers for their valuable suggestions to improve the quality and presentation of the paper.

REFERENCES

(1) Dargahi, J.; Najarian, S. Human tactile perception as a standard for artificial tactile sensing—a review. *Int. J. Med. Rob. Comput. Assisted Surg.* **2004**, *1*, 23−35.

(2) Hoshi, T.; Shinoda, H. In *Robot Skin Based on Touch-Area-Sensitive Tactile Element*, Proceedings 2006 IEEE International Conference on Robotics and Automation; IEEE, 2006.

(3) Kim, H. K.; Lee, S. G.; Han, J. E.; Kim, T. R.; Hwang, S. U.; Ahn, S. D.; You, I. K.; Cho, K. I.; Song, T. K.; Yun, K. S. In*Transparent and Flexible Tactile Sensor for Multi Touch Screen Application with Force Sensing*, International Solid-State Sensors, Actuators and Microsystems Conference;IEEE, 2009.

(4) Miao, P.; Wang, J.; Zhang, C.; Sun, M.; Cheng, S.; Liu, H. Graphene nanostructure-based tactile sensors for electronic skin applications. *Nano-Micro Lett.* **2019**, *11*, No. 71.

(5) Fu, X.; Zhang, J.; Xiao, J.; Kang, Y.; Yu, L.; Jiang, C.; Pan, Y.; Dong, H.; Gao, S.; Wang, Y. A high-resolution, ultrabroad-range and sensitive capacitive tactile sensor based on a CNT/PDMS composite for robotic hands. *Nanoscale* **2021**, *13*, 18780−18788.

(6) Li, Y.; Zheng, L.; Wang, X.; Huang, W. Resistive Tactile Sensors. In *Functional Tactile Sensors*; Elsevier, 2021; pp 13−30.

(7) Bahrami, S.; Moriot, J.; Masson, P.; Grondin, F. *Machine Learning for Touch Localization on Ultrasonic Wave Touchscreen*. 2022, arXiv preprint arXiv:2202.08947. arXiv.org e-Printarchive. https://arxiv.org/abs/2202.08947.

(8) Jin, M.; Jin, M.; Zhang, L.; Yang, R.; Yang, R. Visual Tactile Sensor Based on Infrared Controllable Variable Stiffness Structure. *IEEE Sens. J.* **2021**, *21*, 27076−27083.

(9) Zhu, L.; Wang, Y.; Mei, D.; Wu, X. Highly sensitive and flexible tactile sensor based on porous graphene sponges for distributed tactile sensing in monitoring human motions. *J. Microelectromech. Syst.* **2019**, *28*, 154−163.

(10) Lü, X.; Qi, L.; Hu, H.; Li, X.; Bai, G.; Chen, J.; Bao, W. Ultra-Sensitive Flexible Tactile Sensor Based on Graphene Film. *Micromachines* **2019**, *10*, No. 730.

(11) Jiang, J.; Tu, S.; Fu, R.; Li, J.; Hu, F.; Yan, B.; Gu, Y.; Chen, S. Flexible piezoelectric pressure tactile sensor based on electrospun BaTiO3/poly (vinylidene fluoride) nanocomposite membrane. *ACS Appl. Mater. Interfaces* **2020**, *12*, 33989−33998.

(12) Xie, Y.; Xu, H.; He, X.; Hu, Y.; Zhu, E.; Gao, Y.; Liu, D.; Shi, Z.; Li, J.; Yang, Q.; Xiong, C. Flexible electronic skin sensor based on regenerated cellulose/carbon nanotube composite films. *Cellulose* **2020**, *27*, 10199−10211.

(13) Rosle, M. H.; Wang, Z.; Shiblee, M. N. I.; Ahmed, K.; Furukawa, H.; Hirai, S. Soft Resistive Tactile Sensor based on CNT-PDMS-Gel to Estimate Contact Force. *IEEE Sens. Lett.* **2022**, *6*, 1−4.

(14) Smarandache, F. *Multispace & Multistructure. Neutrosophic Transdisciplinarity (100 Collected Papers of Science)*; Infinite Study, 2010; Vol. *4*.

(15) Afzal, U.; Alrweili, H.; Ahamd, N.; Aslam, M. Neutrosophic statistical analysis of resistance depending on the temperature variance of conducting material. *Sci. Rep.* **2021**, *11*, No. 23939.

(16) Afzal, U.; Ahmad, N.; Zafar, Q.; Aslam, M. Fabrication of a surface type humidity sensor based on methyl green thin film, with the analysis of capacitance and resistance through neutrosophic statistics. *RSC Adv.* **2021**, *11*, 38674−38682.

(17) Afzal, U.; Aslam, M.; Al-Marshadi, A. H. Analyzing imprecise graphene foam resistance data. *Mater. Res. Express* **2022**, *9*, No. 045007.

(18) Afzal, U.; Afzal, J.; Aslam, M. Analyzing the Imprecise Capacitance and Resistance Data of Humidity Sensors. *Sens. Actuators, B* **2022**, *367*, No. 132092.

(19) Afzal, U.; Afzal, F.; Maryam, K.; Aslam, M. Fabrication of flexible temperature sensors to explore indeterministic data analysis for robots as an application of Internet of Things. *RSC Adv.* **2022**, *12*, 17138−17145.
(20) Cho, S. W.; Jeong, J. A.; Bae, J. H.; Moon, J. M.; Choi, K. H.; Jeong, S. W.; Park, N. J.; Kim, J. J.; Lee, S. H.; Kang, J. W.; Yi, M. S.; Kim, H. K. Highly flexible, transparent, and low resistance indium zinc oxide−Ag−indium zinc oxide multilayer anode on polyethylene terephthalate substrate for flexible organic light light-emitting diodes. *Thin Solid Films* **2008**, *516*, 7881−7885.
(21) Soltabayev, B.; Yıldırım, M. A.; Ateş, A.; Acar, S. The effect of indium doping concentration on structural, morphological and gas sensing properties of IZO thin films deposited SILAR method. *Mater. Sci. Semicond. Process.* **2019**, *101*, 28−36.
(22) Kim, H.-K.; Lee, S.; Yun, K.-S. Capacitive tactile sensor array for touch screen application. *Sens. Actuators, A* **2011**, *165*, 2−7.
(23) Chen, Y.; Zhu, J.; Xie, Y.; Feng, N.; Liu, Q. H. Smart inverse design of graphene-based photonic metamaterials by an adaptive artificial neural network. *Nanoscale* **2019**, *11*, 9749−9755.
(24) Maslyczyk, A.; Roberge, J.-P.; Duchaine, V. In *A Highly Sensitive Multimodal Capacitive Tactile Sensor*, International Conference on Robotics and Automation (ICRA); IEEE, 2017.
(25) Ubaid, F.; Ahmad, Z.; Shakoor, R. A.; Mohamed, A. M. A. Surface engineering of the PLA films for fabricating dexterous humidity sensors. *J. Mater. Sci.: Mater. Electron.* **2018**, *29*, 8135−8141.
(26) Maji, D.; Das, S. Analysis of plasma-induced morphological changes in sputtered thin films over compliant elastomer. *J. Phys. D: Appl. Phys.* **2014**, *47*, No. 105401.
(27) Marinho, F.; Carvalho, C. M.; Apolinário, F. R.; Paulucci, L. Measuring light with light-dependent resistors: an easy approach for optics experiments. *Eur. J. Phys.* **2019**, *40*, No. 035801.
(28) Zhu, J.; Cui, Q.; Wen, W.; Zhang, X.; Wang, S. Cu/CuO-Graphene Foam with Laccase-like Activity for Identification of Phenolic Compounds and Detection of Epinephrine. *Chem. Res. Chin. Univ.* **2022**, *38*, 919−927.
(29) Afzal, U.; Aslam, M.; Afzal, F.; Maryam, K.; Ahmad, N.; Zafar, Q.; Farooq, Z. Fabrication of a graphene-based sensor to detect the humidity and the temperature of a metal body with imprecise data analysis. *RSC Adv.* **2022**, *12*, 21297−21308.

https://doi.org/10.1021/acsomega.2c04156
ACS Omega XXXX, XXX, XXX−XXX